Inorganica Chimica Acta 432 (2015) 258–266

Contents lists available at ScienceDirect

Inorganica Chimica Acta

journal homepage: www.elsevier.com/locate/ica

Fe(III) salEen derived Schiff base complexes as potential contrast agents

Bernardo de P. Cardoso [a], Ana I. Vicente [a], Joseph B.J. Ward [b,*], Pedro J. Sebastião [c,d,*], Fabián Vaca Chávez [c,g], Sónia Barroso [e], Alexandra Carvalho [f], Stephen J. Keely [b], Paulo N. Martinho [a,*], Maria José Calhorda [a]

[a] Centro de Química e Bioquímica, DQB, Faculdade de Ciências, Universidade de Lisboa, Campo Grande, 1749-016 Lisboa, Portugal
[b] Molecular Medicine Laboratories, Royal College of Surgeons in Ireland Education and Research Centre, Beaumont Hospital, Beaumont, Dublin 9, Ireland
[c] Condensed Matter Physics Centre, Universidade de Lisboa, Lisbon, Portugal
[d] Departamento de Física, Instituto Superior Técnico, Universidade de Lisboa, Lisbon, Portugal
[e] Centro de Química Estrutural, Instituto Superior Técnico, Universidade de Lisboa, Av. Rovisco Pais, 1049-001 Lisboa, Portugal
[f] CENIMAT-I3N/DCM/FCT/UNL, Campus da Caparica, Caparica, Portugal
[g] Permanent address: FaMAF - Universidad Nacional de Córdoba, IFEG CONICET, X5016LAE Córdoba, Argentina

ARTICLE INFO

Article history:
Received 13 February 2015
Received in revised form 13 April 2015
Accepted 20 April 2015
Available online 2 May 2015

Keywords:
Fe(III) complexes
Evans' method
Contrast agent
NMRD
Cell toxicity

ABSTRACT

Three iron(III) complexes with ligands derived from *N*-ethyl-*N*-(2-aminoethyl)salicylaldiminate (H, **1**; 5-Br, **2**; 3-OMe, **3** substituents at the phenyl group) were prepared and the X-ray crystal structures of **1** and **2** are reported. NMR studies of solutions of these complexes in DMSO allowed for investigation of their magnetic behaviour and paramagnetic relaxation contribution. The relaxivities measured ranged from 0.35 to 0.80 $mM^{-1}\,s^{-1}$ for proton Larmor frequencies from 0.01 to 300 MHz, in agreement with those known for other iron(III) based contrast agents. Biological studies on colonic epithelial T_{84} cell monolayers showed that the compounds exert toxic effects only at concentrations higher than 100 μM while coincidently reducing colonic epithelial secretory function. These two features make these complexes good candidates for further development in order to be used as MRI contrast agents.

1. Introduction

Magnetic Resonance Imaging (MRI) is a widely used technique for visualising anatomical soft tissue, using non-ionising radiation and displaying excellent spatial resolution [1]. However, it has a limited sensitivity when compared with other imaging techniques (e.g. optical or nuclear) [2,3], due to the abundance of the water signal monitored [4]. Thus, efforts to improve this shortcoming focus mainly on chemical substances which enhance MRI contrast [5].

The field of MRI contrast agents has been dominated by trivalent gadolinium (Gd^{3+}) complexes [5–8] as they are paramagnetic with seven unpaired electrons [5]. However, concerns regarding Gd^{3+} toxicity [9–11] are directing research towards the use of other metals as paramagnetic contrast agents. This resulted in an expansion of non-lanthanide based contrast agents (e.g.: Mn(II) [12–16], Fe(II)/Fe(III) [17–24], Co(II)/Co(III) [25,26] and Ni(II) [27]). Among these, iron is a biocompatible metal and paramagnetism is observed for high-spin (HS) Fe(II) and both high-spin and low-spin (LS) Fe(III) octahedral species [28,29]. Recently, the approaches to iron based contrast agents focused on either design of molecular compounds [19,23] or development of nanoparticles [14,30,31].

Schiff bases were shown to be a versatile class of ligands for coordination chemistry [32]. These ligands can be tailored to contain groups bearing labile protons (e.g. OH or NH) thus increasing the solvent NMR relaxivity (r) produced by the contrast agent. This enhancement is magnetic field dependent and the parameters that describe the paramagnetic relaxation can be obtained, for instance, through a magnetic field dependence of the spin-lattice relaxivity (r_1) study usually called Nuclear Magnetic Relaxation Dispersion (NMRD) [16]. This effect is observed by measuring solvent spin-lattice relaxation rates over a broad range of magnetic fields corresponding to proton Larmor frequencies ($\nu_{L,H}$) from 10 kHz to hundreds of MHz, in general.

We have been investigating this class of ligands aiming at finding new examples of paramagnetic systems using Fe(III) [33]. Given that these complexes contain iron and have protons that can easily exchange with the solvent we decided to investigate their potential as contrast agents.

Administration of contrast agents is commonly done either orally or intravenously. Ingested contrast agents will, inevitably, come into contact with the epithelial lining of the gastrointestinal (GI) tract. The GI epithelial barrier is a monolayer of cells that

* Corresponding authors at: Condensed Matter Physics Centre, Universidade de Lisboa, Lisbon, Portugal (P.J. Sebastião).
E-mail addresses: seosamh.ward@gmail.com (J.B.J. Ward), pedro.jose.sebastiao@tecnico.ulisboa.pt (P.J. Sebastião), pnmartinho@fc.ul.pt (P.N. Martinho).

http://dx.doi.org/10.1016/j.ica.2015.04.026
0020-1693/

serves several key functions, such as the transporting of fluid and electrolytes to and from the gut lumen. The absorption and secretion of fluids across the epithelial barrier is driven by osmotic gradients, which in turn are generated by the active transport of ions. Cl^- secretion, the primary driving force for fluid secretion, is promoted by hormones and neuroimmune agonists, which bind to cell surface receptors and increase cytosolic second messengers, most notably cyclic AMP (cAMP) and Ca^{2+}. These second messengers then interact with the transport proteins of the Cl^- secretory pathway to stimulate fluid secretion into the gut lumen [34]. Employing the newly synthesised potential contrast agents, we show their effects on colonic epithelial cell survival and function.

Here we report the synthesis of compounds of the general formula $[Fe(R\text{-}salEen)_2]Cl$ (salEen = *N*-ethyl-*N*-(2-aminoethyl)salicylaldiminate; R = H, **1**; 5-Br, **2**; 3-OMe, **3**) and present the X-ray crystal structures for both $[Fe(H\text{-}salEen)_2]Cl{\cdot}0.5H_2O$ (**1**) and $[Fe(Br\text{-}salEen)_2]Cl{\cdot}0.5H_2O$ (**2**). The magnetic behaviour in solution assessed by the Evans' method [35], NMRD profiles in DMSO solutions, cell toxicities and their effects on Cl^- secretion.

2. Experimental

2.1. Syntheses

N-ethylethylenediamine, salicylaldehyde, 5-bromosalicylaldehyde, *o*-vanillin, iron(III) chloride hexahydrate, iron(II) chloride and all the solvents were purchased and used without further purification. IR transmittance spectra were obtained on a Nicolet Nexus 6700 FTIR spectrophotometer in the 400–4000 cm^{-1} range with 4 cm^{-1} resolution using KBr pellets.

2.1.1. $[Fe(salEen)_2]Cl{\cdot}xH_2O$ (**1·xH₂O**)

Salicylaldehyde (214 μL, 2 mmol) was added to a solution of *N*-ethylethylenediamine (210 μL, 2 mmol) in methanol (30 mL) and left stirring for 15 minutes. Iron(III) chloride hexahydrate (270 mg, 1 mmol) was added to the previous mixture and left stirring for 1 h. The mixture was filtered and needle shaped dark brown crystals of **1·0.5H₂O** were obtained by slow evaporation in methanol (81 mg, 14%). IR (KBr): ν_{max}/cm^{-1} 3095 (ν_{NH}, m), 2924–2853 (ν_{CH}, m), 1629 ($\nu_{C=N}$, s), 1598 ($\delta_{C=C}$, m), 1296 (ν_{C-N}, s). Anal. found (calcd) for $C_{22}H_{34}ClFeN_4O_4{\cdot}2H_2O$: C 51.99 (51.83); H 6.32 (6.72); N 10.95 (10.99).

2.1.2. $[Fe(5\text{-}Br\text{-}salEen)_2]Cl{\cdot}xH_2O$ (**2·xH₂O**)

The same procedure as for the synthesis of compound **1** was used, starting from *N*-ethylethylenediamine (210 μL, 2 mmol) in methanol (30 mL), 5-bromosalicylaldehyde (402 mg, 2 mmol) and iron(II) chloride (127 mg, 1 mmol). The mixture was filtered and needle shaped dark brown crystals of **2·0.5H₂O** were obtained by slow evaporation in methanol (85 mg, 13%). IR (KBr): ν_{max}/cm^{-1} 3078 (ν_{NH}, m), 2970–2858 (ν_{CH}, m), 1633 ($\nu_{C=N}$, s), 1590 ($\delta_{C=C}$, m), 1295 (ν_{C-N}, s). Anal. found (calcd) for $C_{24}H_{32}Br_2ClFeN_4O_4{\cdot}2H_2O$: C 39.09 (39.52); H 4.33 (4.57); N 8.22 (8.38).

2.1.3. $[Fe(3\text{-}OMe\text{-}salEen)_2]Cl$ (**3**)

The same procedure used to synthesise compound **1** was used for compound **3** synthesis, starting from *N*-ethylethylenediamine (210 μL, 2 mmol) in methanol (30 mL), *o*-vanillin (304 mg, 2 mmol) and iron(II) chloride (127 mg, 1 mmol). A dark green microcrystalline solid was filtered, washed with methanol and dried under vacuum (116 mg, 20%). IR (KBr): ν_{max}/cm^{-1} 3063 (ν_{NH}, m), 2994–2831 (ν_{CH}, w), 1633 ($\nu_{C=N}$, s), 1598 ($\delta_{C=C}$, m), 1308 (ν_{C-N}, s). Anal. found (calcd) for $C_{24}H_{34}ClFeN_4O_4$: C 53.48 (53.89); H 6.50 (6.60); N 10.39 (10.48).

2.2. General procedures for X-ray crystallography

Crystals suitable for single-crystal X-ray analysis were obtained for **1·0.5H₂O** and **2·0.5H₂O,** as described in the synthetic procedures. The data were collected using graphite monochromated Mo Kα radiation (λ = 0.71073 Å) on a Bruker AXS-KAPPA APEX II diffractometer equipped with an Oxford Cryosystem open-flow nitrogen cryostat. Cell parameters were retrieved using Bruker SMART software and refined using Bruker SAINT on all observed reflections. Absorption corrections were applied using SADABS [36]. The structures were solved and refined using direct methods with program SIR2004 [37] using WINGX-Version 1.80.01 [38] SHELXL [39,40] system of programs. All non-hydrogen atoms were refined anisotropically and the hydrogen atoms were inserted in idealised positions and allowed to refine riding on the parent carbon atom. The molecular diagrams were drawn with ORTEP-3 for Windows [41] included in the software package.

Both structures refined to a good convergence, even though crystals of **2·0.5H₂O** were of poor quality presenting low ratio of observed/unique reflections. SIMU and ISOR restraints were applied in order to prevent some atoms from turning non-positive-definite.

It was not possible to locate the hydrogen atoms of the H_2O molecules in both structures of **1·0.5H₂O** and **2·0.5H₂O**.

Flack parameter *x* obtained for **2·0.5H₂O** is meaningless (0.44(2)). The crystal is most likely a 50/50 inversion twin. No absolute configuration determination is possible. For crystallographic experimental data and structure refinement parameters see Table 1. Data for structures **1** and **2** were deposited in CCDC under the deposit numbers CCDC 1018927–1018928 and can be obtained free of charge from The Cambridge Crystallographic Data Centre via www.ccdc.cam.uk/data_request/cif.

2.3. NMR studies

2.3.1. Evans' method

Magnetic measurements of complexes **1** and **2** in solution were performed at room temperature (rt) by ^1H NMR using the Evans' method [35] on a Bruker Avance 400 spectrometer operating at 400.14 MHz at a constant temperature of 298.15 K. The measurements for each compound at different concentrations ([*c*] = 100,

Table 1
Selected crystallographic experimental data and structure refinement parameters for **1·0.5H₂O** and **2·0.5H₂O**.

	1·0.5H₂O	**2·0.5H₂O**
Empirical formula	$C_{44}H_{60}Cl_2Fe_2N_8O_5$	$C_{44}H_{56}Br_4Cl_2Fe_2N_8O_5$
Formula weight	963.60	1279.21
T (K)	150(2)	150(2)
Crystal system	orthorhombic	monoclinic
Space group	*Fdd*2	$P2_1$
a (Å)	18.230(4)	10.282(2)
b (Å)	53.905(11)	25.841(6)
c (Å)	9.8130(18)	10.606(2)
α (°)	90	90
β (°)	90	116.136(10)
γ (°)	90	90
V (Å^3)	9643(3)	2529.8(9)
Z, ρ_{calc} (g cm^{-3})	8, 1.327	2, 1.679
μ(mm^{-1})	0.763	3.889
Crystal size	0.12 × 0.12 × 0.04	0.20 × 0.04 × 0.04
Crystal colour	brown	brown
Crystal shape	plate	prism
Refl. collected	26883	21449
Unique refl. [*R*(int)]	4187 [0.0984]	7157 [0.0989]
R_1 [$I > 2\sigma(I)$]	0.0591	0.0845
wR_2 [$I > 2\sigma(I)$]	0.1207	0.2011
GooF	1.046	1.043

50, 10 and 5 mM) were performed in standard 5 mm NMR tubes containing the paramagnetic samples dissolved in DMSO-d_6 with an inert reference of 0.03% TMS, against a reference insert tube filled with the same solvent (0.03% TMS in DMSO-d_6) and their shift measured in Hz.

2.3.2. NMRD measurements

The proton spin–lattice relaxation time, T_1, was measured over $\nu_{L,H}$, range from 10 kHz to 300 MHz. In the range 10 kHz–8.9 MHz, the data were obtained with a home-developed fast field-cycling (FFC) relaxometer operating with a polarization and detection fields of 0.215 T and a switching time less than 3 ms [42]. For frequencies between 10 and 91 MHz, a variable-field iron-core magnet and a 300 MHz Bruker Avance II spectrometer were used and T_1 was measured applying the inversion recovery sequence.

2.3.3. Self-diffusion measurements

The diffusion coefficient, D, expressed in $m^2\ s^{-1}$, was measured using the stimulated spin-echo sequence [43] on a Bruker Avance II 300 MHz spectrometer equipped with a Diff 30 gradient unit. D was obtained from the echo decay using the stimulated echo sequence according to

$$I = I_0 \exp[-\gamma^2 g^2 \delta^2 D(\Delta - \delta/3)] \quad (1)$$

where γ is the proton's gyromagnetic ratio, g is the magnetic field gradient strength, δ = 1 ms is the gradient pulse length, Δ = 20 ms is the delay between the gradients pulses.

2.4. Biological essays

2.4.1. Sample preparation

Stock solutions (1 M) of compounds **1–3** were prepared by dissolving these in non-anhydrous DMSO. Solutions of different concentrations (1 nM, 100 nM, 10 μM, 100 μM and 500 μM) were further prepared by dissolving aliquots of the stock solution in Ringer's solution containing (in mM): 40 Na^+, 5.2 K^+, 1.2 Ca^{2+}, 1.2 Mg^{2+}, 119.8 Cl^-, 25 HCO_3^-, 0.4 $H_2PO_4^-$, 2.4 HPO_4^{2-}, and 10 glucose.

2.4.2. Electrophysiological measurements

T_{84} cell monolayers, cultured as previously described [44], were mounted in Ussing chambers (aperture = 0.6 cm^2), voltage-clamped to zero potential difference and bathed in Ringer's solution, and monitored for changes in short circuit current (ΔI_{sc}) using a VCC MC8 Voltage Clamp (Physiological Instruments, San Diego, CA). Under such conditions secretagogue-induced ΔI_{sc} reflect changes in electrogenic Cl^- secretion [45]. Results were normalised and expressed as ΔI_{sc} (μA cm^{-2}).

2.4.3. Transepithelial electrical resistance (R_{te}) measurements

R_{te}, Ω cm^2 used as a measure of intestinal epithelial barrier integrity was measured directly using an epithelial volt meter (EVOM2).

2.4.4. Lactate dehydrogenase (LDH) assay

Lactate dehydrogenase (LDH) release, used as a measure of toxicity, from T_{84} intestinal epithelial cells, was measured using a commercially available kit (Sigma–Aldrich, Gillingham, UK). T_{84} cell monolayers were cultured on permeable supports for 7–14 days until the R_{te} had stabilised. Cells were then treated bilaterally with compounds **1–3** for 24 h. Following this, equal aliquots of apical and basolateral culture media were analysed for the presence of LDH by spectrophotometry.

2.4.5. Statistical analysis

All biological data are expressed as mean ± standard error of the mean (sem) for a series of n experiments. Student's t-test was used to compare paired data. One-way analysis of variance with the Student–Newman–Keuls (SNK) multiple comparisons post-test was used when three or more groups of data were compared. p values $\leqslant 0.05$ were considered to be statistically significant.

2.5. Stability tests in aqueous solutions

The stability of aqueous solutions of complexes **1–3** was followed by UV–Vis and NMR. UV–Vis spectra of a 1×10^{-4} mol L^{-1} aqueous solution of $[Fe(H_2O)_6]^{3+}$, the three compounds in DMSO (1×10^{-4} mol L^{-1}) and the three complexes in H_2O (obtained by dilution of a 1×10^{-3} mol L^{-1} stock DMSO solution with H_2O to 1×10^{-4} mol L^{-1}) were recorded on a Shimadzu 50/60 Hz spectrometer. The aqueous solutions of the three complexes were recorded at t = 0 h, t = 24 h, t = 48 h and t = 196 h. NMR spectra of the three complexes were also recorded in DMSO-d^6 and in a mixture of DMSO-d^6/D_2O (70/30). NMR studies were carried out for all three compounds at times t = 0 h, t = 24 h and t = 196 h. Stability studies show that the most stable compound to hydrolysis is by far complex **2** and the least stable complex **1**. These studies can be found in the Supplementary information.

3. Results and discussion

3.1. Syntheses

The synthesis of complexes **1–3** was made as described in Scheme 1. Complex **1** was first reported by Clément et al. [46] and **1·*x*H$_2$O** is now reported. Complex **2** was synthesised with crystallisation water molecules (**2·*x*H$_2$O**) and complex **3** was obtained in its unsolvated form. The complexes were characterised by elemental analysis, IR and complexes **1·0.5H$_2$O** and **2·0.5H$_2$O** were also structurally characterised by single crystal X-ray diffraction. The IR spectra of all three complexes presented the characteristic C=N stretching band at 1633 cm^{-1}, which confirms the successful formation of the imine. Furthermore, the IR spectra of both **1·*x*H$_2$O** and **2·*x*H$_2$O** indicate the presence of water molecules (Figs. S2 and S3)

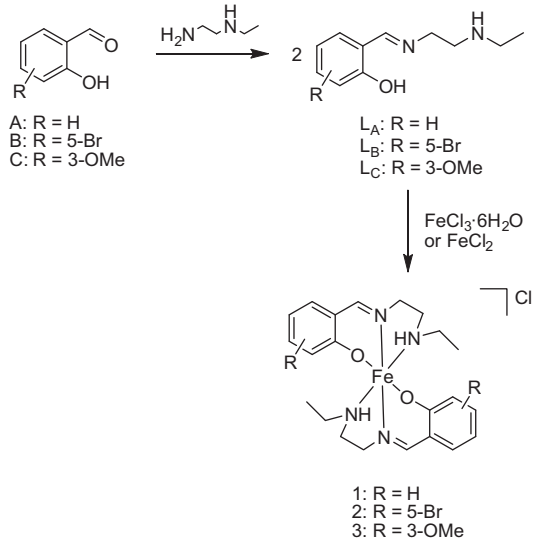

Scheme 1. General method used in the synthesis of complexes **1–3**.

3.2. X-ray studies

Complex **1** crystallises in the orthorhombic system, space group *F*dd2, with one $[Fe(salEen)_2]^+$ cation, one Cl^- anion and half a water molecule in the asymmetric unit. An ORTEP view of **1·0.5H$_2$O** is depicted in Fig. 1 and selected bond distances and angles (data obtained at 150 K) are listed in Table 2. The iron(III) is octahedrally coordinated by two oxygen, two nitrogen(amine) and two nitrogen(imine) atoms belonging to two salEen ligands bound in the meridional coordination mode. The Fe–O bond lengths (1.885(4) and 1874(4) Å) are shorter than the Fe–N(imine) (1.917(5) and 1.927(5) Å) distances, which are shorter than the Fe–N(amine) ones (2.036(5) and 2.069(5) Å). Compared to the literature, these values suggest a LS Fe(III) centre [33,47–50].

The crystal structure of **1·0.5H$_2$O** comprises alternating layers of $[Fe(salEen)_2]^+$ cations and Cl^- anions parallel to the *ac* plane with H_2O molecules located in the void spaces (Fig. 2). The layers are interconnected through short intermolecular contacts between neighbouring cations and through hydrogen bonds between the amine groups of the salEen cations and the Cl^- anions (N1–H1···Cl1 and N3–H3···Cl1, *d*(D···A) = 3.269(6) and 3.192(6) Å, respectively).

Complex **2** crystallises in the monoclinic system, space group $P2_1$, with two $[Fe(salEen)_2]^+$ cation, two Cl^- anions, and one water molecule in the asymmetric unit. An ORTEP view of **2·0.5H$_2$O** (only one of the molecules, *molecule 1*, and the co-crystallised water molecule are shown) is depicted in Fig. 3 and selected bond distances and angles for both *molecules 1* and *2* (data obtained at 150 K) are listed in Table 2. Similarly to **1·0.5H$_2$O**, the coordination around each iron(III) centre is distorted octahedral with two salEen ligands bound in the meridional coordination mode. In both *molecules 1* and *2*, the Fe–O bond lengths are shorter than the Fe–N(imine) distances, which are shorter than the Fe–N(amine) as observed for complex **1**. Although *molecules 1* and *2* are very similar, they are crystallographically different: the Fe–O and Fe–N bond distances are longer in *molecule 2* than in *molecule 1*. The values observed for these molecules suggest a LS Fe(III) centre in *molecule 1* and a HS Fe(III) centre in *molecule 2* [33,47–50].

The crystal packing of **2·0.5H$_2$O** depicted in Fig. 4 shows alternating layers of $[Fe(salEen)_2]^+$ cations and Cl^- anions parallel to the *ac* plane. Co-crystallised H_2O molecules are located between the Cl^- anions. As observed in the structure of **1·0.5H$_2$O** the layers

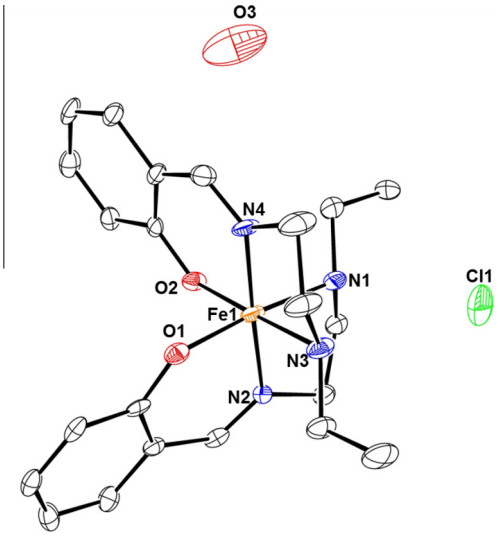

Fig. 1. ORTEP-3 diagram of **1·0.5H$_2$O** with co-crystallised H_2O, using 30% probability level ellipsoids. Hydrogen atoms are omitted for clarity.

Table 2
Selected bond lengths (Å) and angles (°) for **1·0.5H$_2$O** and **2·0.5H$_2$O**.

	1·0.5H$_2$O	**2·0.5H$_2$O** *molecule 1*	*molecule 2*
Fe(1)–O(1)	1.885(4)	1.866(11)	1.955(12)
Fe(1)–O(2)	1.874(4)	1.870(12)	1.938(12)
Fe(1)–N(1)	2.069(5)	2.048(13)	2.192(14)
Fe(1)–N(2)	1.927(5)	1.939(13)	2.077(17)
Fe(1)–N(3)	2.036(5)	2.052(15)	2.223(14)
Fe(1)–N(4)	1.917(5)	1.903(15)	2.097(15)
O(2)–Fe(1)–O(1)	93.1(2)	93.2(5)	94.9(5)
O(2)–Fe(1)–N(4)	93.4(2)	95.0(6)	86.4(5)
O(1)–Fe(1)–N(4)	89.1(2)	85.5(5)	93.7(5)
O(2)–Fe(1)–N(2)	86.7(2)	86.6(5)	96.0(6)
O(1)–Fe(1)–N(2)	93.4(2)	93.7(5)	87.9(6)
N(4)–Fe(1)–N(2)	177.6(2)	178.2(6)	177.0(6)
O(2)–Fe(1)–N(3)	177.4(2)	177.6(5)	163.8(5)
O(1)–Fe(1)–N(3)	86.7(2)	88.4(6)	94.2(6)
N(4)–Fe(1)–N(3)	84.1(2)	83.3(6)	79.7(6)
N(2)–Fe(1)–N(3)	95.9(2)	95.1(6)	97.7(6)
O(2)–Fe(1)–N(1)	89.1(2)	86.9(5)	88.6(5)
O(1)–Fe(1)–N(1)	175.3(2)	177.0(5)	165.5(5)
N(4)–Fe(1)–N(1)	95.0(2)	97.5(5)	100.6(5)
N(2)–Fe(1)–N(1)	82.6(2)	83.3(5)	77.7(6)
N(3)–Fe(1)–N(1)	91.3(2)	91.6(6)	86.0(6)

are interconnected through short intermolecular contacts between neighbouring cations and through hydrogen bonds between the amine groups of the salEen cations and the Cl^- anions (N1-H1···Cl1 and N3-H3···Cl1). The H_2O molecule is hydrogen bonded to both anions of *molecules 1* and *2* (Table 3).

DFT calculations (Gaussian09 [51], PBE0 [52,53], 6-31G** [54–58] and sdd + polarization for Fe) were performed in order to estimate the energy difference between the HS and the LS forms of complexes **1** and **2**, using three models in the geometry optimization: the cation, the cation with two N–H···Cl hydrogen bonds, and this salt with one water molecule hydrogen bonded to the chloride ion (O–H···Cl). The introduction of the chloride modifies the bond lengths by ~0.01–0.07 Å, while the effect of the water molecule is even smaller. The second model (cation and chloride) gives the best agreement with the experimental distances (details, Table S1 and Fig. S5 in supplementary material). For this model of complex **2**, the Fe–O distances are 1.945 (HS) and 1.887 Å (LS), the Fe–N(imine) distances 2.123 (HS) and 1.931 Å (LS), and the Fe–N(amine) distances 2.207 (HS) and 2.041 Å (LS), in good agreement with the distances observed in *molecule 1* (LS) and *molecule 2* (HS) and their assignment. The HS–LS energy difference is 0.7 kcal mol^{-1} lower for complex **2**. It is thus more likely to find the coexistence of the two structures in complex **2**. On the other hand, the model is very simple and the value is indicative.

3.3. NMR studies

The magnetic behaviour in solution at rt of all three complexes was assessed by NMR spectroscopy (magnetic molar susceptibility-χ_m and spin lattice relaxation time-T_1). Unfortunately the solubility of compound **3** did not allow a correct determination of both $\chi_m T$ and T_1 values.

$\chi_m T$ values determined by the Evans' method (Table 4, Fig. S6) show that at different concentrations their values remain practically constant, with $\chi_m T$ changing from an average value of 4 cm^3 mol^{-1} K for compound **1** to **3** cm^3 mol^{-1} K for compound **2**. Taking into account the spin only values for an octahedral Fe(III) complex for both HS and LS configurations we can conclude that while compound **1** is essentially HS (≈ 90%), compound **2** shows a mixture of spin states (HS ≈ 64%). A similar ring substituent effect has been reported by Tweedle and Wilson [59] and was also recently observed by our group [33].

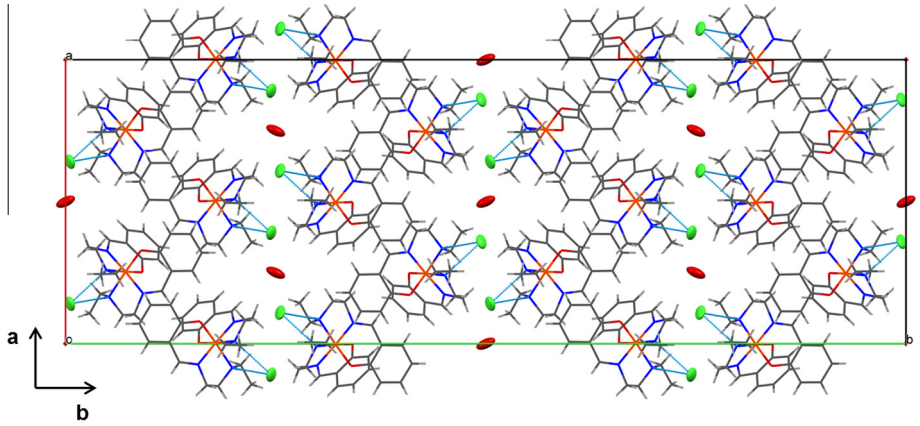

Fig. 2. Mercury packing diagram of **1·0.5H$_2$O** viewed along the *c* axis showing the layers of $[Fe(salEen)_2]^+$ cations alternating with Cl^- anions and H_2O molecules. Hydrogen bonds between the amine groups of the salEen cations and the Cl^- anions are represented as light blue dashed lines.

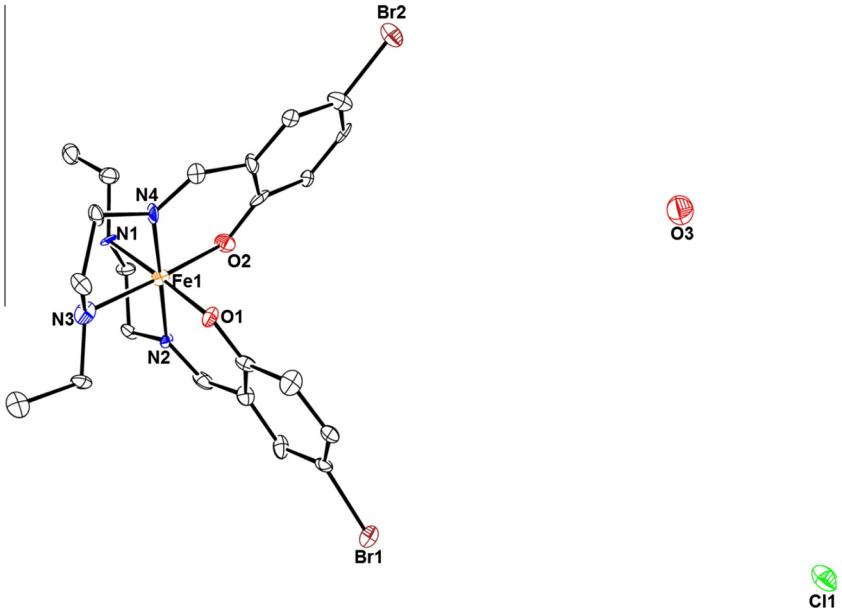

Fig. 3. ORTEP-3 diagram of **2·0.5H$_2$O** (*molecule 1*) with co-crystallised H_2O, using 30% probability level ellipsoids. Hydrogen atoms are omitted for clarity.

To assess the potential of the complexes as MRI contrast agents, we used NMRD to determine their proton spin-lattice relaxivity enhancement effect (r_1) and to gain insight into the relaxation mechanisms of the solvent molecules. The source of relaxation increase is the modulation by dynamics of the intermolecular dipole-dipole interaction between the nuclear spin moment of the solvent molecules and the electron magnetic moment of the magnetic species [16].

In general, the experimental measured T_1 can be written as

$$\frac{1}{T_1} = \frac{1}{T_1 d} + r_1[c] \tag{2}$$

where T_{1d} is the observed relaxation time of the solvent (DMSO) in the absence of paramagnetic molecules (s), [*c*] is the concentration of the ionic species (mM). r_1 measures the efficiency of the agent referred to 1 mM concentration and it is expected to be concentration independent ($mM^{-1}\ s^{-1}$) [60].

^1H T_1 can be affected by the presence of magnetic ions in two ways: (i) the so-called inner-sphere (*is*) relaxation, associated to the protons bound temporarily to ions or ion complexes, and (ii) the outer-sphere (*os*) relaxation, which applies to protons that move or diffuse close to magnetic ions or particles [61][16]. Then, the relaxivity defined in Eq. (2) can be written as the sum of the two contributions

$$r_1 = r_1^{is} + r_1^{os} \tag{3}$$

Fig. 5 shows r_1 at three different concentrations (1, 10 and 100 mM) for complex **2**, using Eq. (2) with $T_{1d} = 0.52\ s^{-1}$ for a reference sample of DMSO. For 100 mM the best match with the other two r_1 data sets was obtained using a different concentration, $[c'] = 35$ mM.

The inset in Fig. 5 shows the relaxation rate ($1/T_1$) for the three different concentrations studied. A clear effect on total measured relaxation rate is observed with increasing concentration.

Fig. 6 shows the results of $1/T_1$ vs. [*c*] for compound **2**, **[2]**, in the range 0–10 mM at three different $\nu_{L,H}$ (100 kHz, 41 MHz and 300 MHz). A clear linear dependence is observed, thus r_1 can be obtained using Eq. (2). The inset plot also shows the values of $1/T_1$ at 100 mM where a clear deviation from the linear dependency is observed. This deviation justifies the use of [*c*′] to obtain

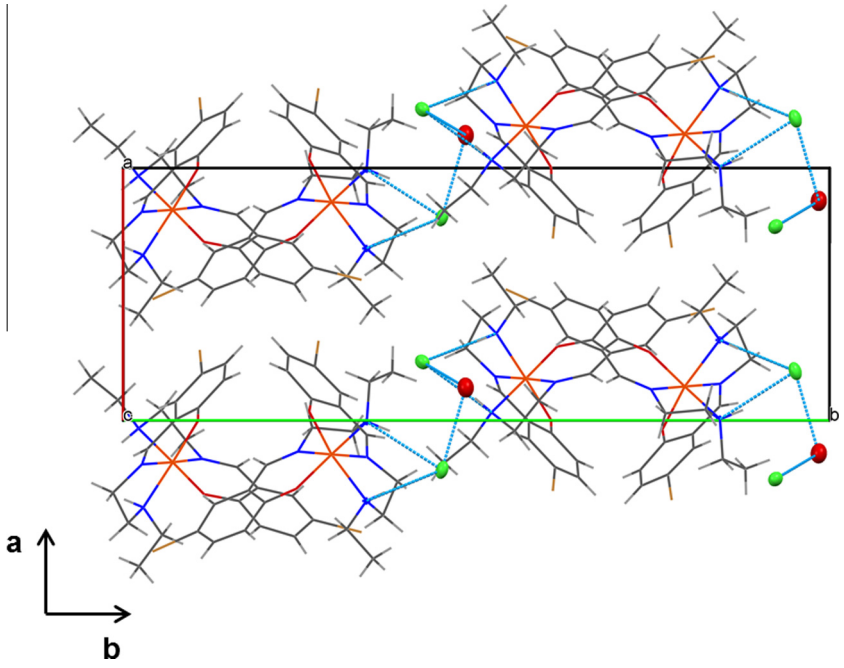

Fig. 4. Mercury packing diagram of **2·0.5H$_2$O** viewed along the *c* axis, showing the layers of $[Fe(salEen)_2]^+$ cations alternating with Cl^- anions and H_2O molecules. Hydrogen bonds between the amine groups of the salEen cations and the Cl^- anions are represented as light blue dashed lines. (For interpretation of the references to colour in this figure legend, the reader is referred to the web version of this article.)

Table 3
Hydrogen bonds between the cationic and anionic layers in **1·0.5H$_2$O** and **2·0.5H$_2$O**.

D–H···A	Distance (Å)			Angle (°)
	D···H	H···A	D···A	D–H···A
1·0.5H$_2$O				
N(1)–H(1)···Cl(1)	0.91	2.36	3.269(6)	177
N(3)–H(3)···Cl(1)	0.91	2.28	3.192(6)	177
2·0.5H$_2$O				
molecule 1				
N(1)–H(1)···Cl(1)	0.91	2.32	3.227(16)	171
N(3)–H(3)···Cl(1)	0.91	2.38	3.264(18)	163
O(3)···Cl(1)			3.251	
molecule 2				
N(1)–H(1)···Cl(1)	0.91	2.34	3.220(16)	162
N(3)–H(3)···Cl(1)	0.91	2.42	3.286(19)	159
O(3)···Cl(1)			3.141	

r_1 dispersion in Fig. 5. These r_1 values are on the same order of magnitude respect to other Fe(III) complexes reported by Richardson et al. [23].

The fact that r_1 dispersions for 1, 10 and 100 mM in Fig. 5 show some differences suggests that deviations from Eq. (2) might be expected.

Fig. 7 shows the fit of the 1 mM solution for **2** using Eq. (2) with both models for *is* and *os* for paramagnetic complexes [16]. Details on the relaxation models and fitting parameters are presented in the Supplementary material [62]. From the *is* model the value obtained for the distance between a Fe^{3+} ion and a communicating DMSO molecule was $r_{FeH} = 4.70 \pm 0.07$ Å. From the contribution of the *os* model, the minimum distance for the interaction between an Fe^{3+} ion and an interacting DMSO molecule was found to be $R_{FeH} = 22 \pm 1$ Å. This distance was obtained from the measured diffusion constant of the DMSO molecules $D = 7.1 \times 10^{-10}$ m^2 s^{-1}, which is slightly smaller than $D = 7.4 \times 10^{-10}$ m^2 s^{-1} of the pure solvent. Additionally the correlation time of the electronic zero-field-splitting (ZFS) relaxation $\tau_v = 1.2 \pm 0.2$ ps, and the mean squared fluctuation of the ZFS $\Delta^2 = (4.8 \pm 0.2) \times 10^{20}$ s^{-2} were estimated from the fitting parameters.

The r_1 dispersions for the two remaining concentrations (10 and 100 mM) were also fitted using the same model obtaining different values for τ_v and for the correlation time associated with the inner sphere relaxation, τ_{mH} (see Supplementary material). As a consequence, the *is* and *os* paramagnetic relaxation contributions are affected, pointing to a possible state of aggregation of individual molecules.

Table 4
$\chi_m T$ values obtained from ^{1}H NMR results in DMSO-d$_6$ for **1** and **2** at rt.

[*c*] (mM)	$\chi_m T$ (cm^3 mol^{-1} K)	
	1 (R = H)	**2** (R = 5-Br)
5	3.7	3.0
10	4.1	3.1
50	4.1	2.8
100	–*	2.9

* Several attempts gave irreproducible results.

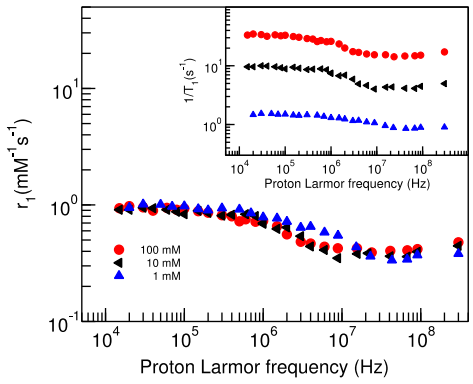

Fig. 5. r_1 dependence with ν_{LH} at concentrations 1, 10 and 100 mM for compound **2**. The inset shows the relaxation rate for the same samples.

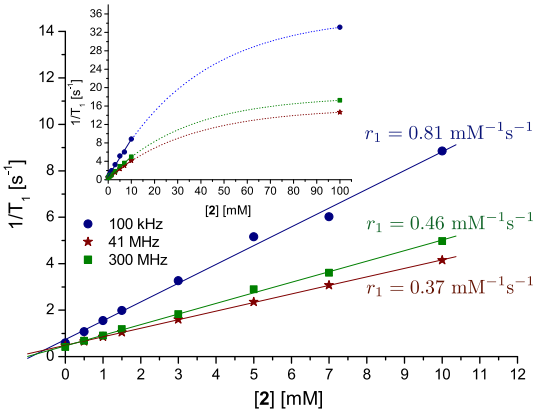

Fig. 6. $1/T_1$ vs **[2]** at three different $\nu_{L,H}$ (100 kHz, 41 MHz and 300 MHz) and the corresponding r_1 values. The inset plot also shows the values of $1/T_1$ for 100 mM where a clear deviation from the linear behaviour is observed. The dotted lines are a guide for the eyes.

3.4. Biological tests

According to the NMR studies these compounds show potential as MRI contrast agents and it is important to estimate their toxicity and effect on cell regulation.

Treatment of T_{84} cells with the compounds **1**–**3** for 24 h resulted in varying degrees of LDH release. Of the three compounds studied, compound **3** was the least toxic and significantly increased LDH release from T_{84} monolayers only at concentrations of 1 mM (see Supplementary material). Compound **1** was the second most toxic, causing a small, but significant, increase in LDH release at 500 μM (see Supplementary material). Compound **2** was the most toxic causing a high degree of cell lysis at 500 μM (Fig. 8). Overall, these complexes exert toxic effects only at high concentrations.

Having ascertained that each of the three compounds caused LDH release when used at high concentrations, we next wished to determine whether the compounds caused a concomitant reduction in barrier function, measured as R_{te}. Compound **3** (500 μM, 24 h) reduced R_{te} to 430.7 Ω cm^2 compared to controls (812.5 Ω cm^2) (n = 4–8, $p \leqslant 0.01$). Similarly to **3**, compound **1** (500 μM, 24 h) reduced R_{te} to 599.1 ± 58.6 Ω cm^2 compared to controls (1155.3 ± 42.2 Ω cm^2; n = 5–6, $p \leqslant 0.001$), whereas compound **2** (500 μM, 24 h) abolished R_{te}, while compound **2** (100 μM, 24 h) reduced R_{te} to 371.7 ± 55.6 μ cm^2 compared to control (889.2 ± 59.5 Ω cm^2; n = 4–8, $p \leqslant 0.01$). Thus the compounds analysed reduce R_{te} across T_{84} colonic epithelial monolayers at concentrations greater than 10 μM.

Following barrier function measurements we went on to determine whether the compounds altered transepithelial Cl^- secretion

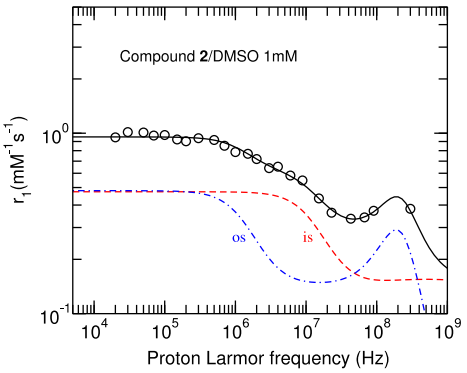

Fig. 7. Fit of the r_1 dispersion for 1 mM of compound **2** using Eqs. (2) and (3). The contributions of the *is* (dashed) and *os* (dash dot) to the total r_1 are also shown.

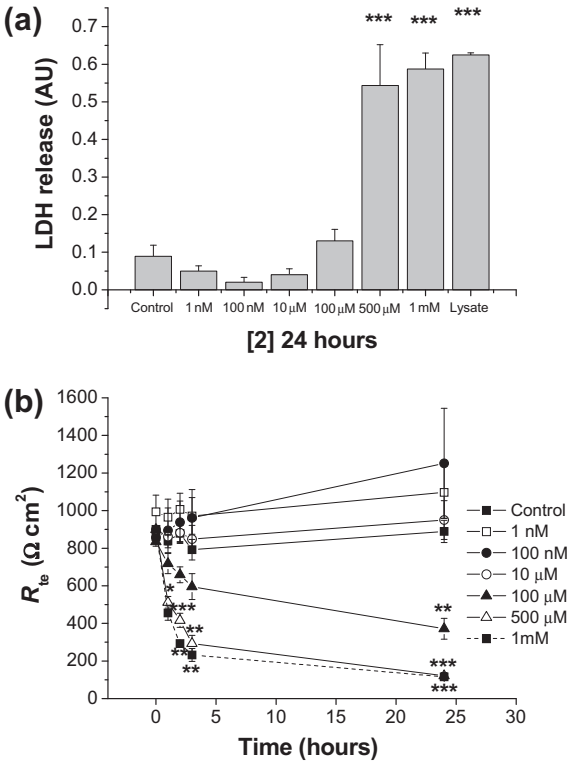

Fig. 8. High concentrations of compound **2** exert toxic effects on T84 monolayers. (a) T_{84} monolayers were treated bilaterally with compound **2** for 24 h. An equal aliquot of apical and basolateral medium was used to measure LDH release from the cells (n = 4–8). (b) T_{84} monolayers were treated with compound **2** at various concentrations (1 nM to 1 mM) over a 24 h period during with R_{te} was measured (n = 4–8).

across T_{84} monolayers, a primary function of colonic epithelial cells. Pre-treatment of T_{84} cell monolayers with the compounds **1**–**3** for 24 h significantly attenuated subsequent Cl^- secretory responses to the Ca^{2+}- and cAMP-dependent secretagogues, carbachol (CCh) and forskolin (FSK), Fig. 9. In **3** (500 μM)-treated monolayers, peak responses to CCh and FSK were 46.4 ± 2.6 μA cm^{-2} (n = 4–8; ns) and 45.8 ± 6.7 μA cm^{-2} (n = 4–8; $p \leqslant 0.01$) compared to those in control cells of 76.2 ± 12.7 μA cm^{-2} and 100.5 ± 13.0 μA cm^{-2}, respectively. In **1** (500 μM)-treated monolayers, peak responses to CCh and FSK were 45.3 ± 8.8 μA cm^{-2} (n = 6; ns) and 55.6 ± 5.6 μA cm^{-2} (n = 6; $p \leqslant 0.001$) compared to those in control cells of 74.2 ± 11.0 μA cm^{-2} and 135.8 ± 9.5 μA cm^{-2} respectively. Finally, in **2** (100 μM)-treated monolayers, peak responses to CCh and FSK were 32.5 ± 6.3 μA cm^{-2} (n = 6–8; ns) and 47.0 ± 4.6 μA cm^{-2} (n = 6–8; $p \leqslant 0.05$) compared to those in control cells of 86.2 ± 18.8 μA cm^{-2} and 107.1 ± 15.3 μA cm^{-2} respectively. The effects of compounds **1**–**3** were concentration–dependent with anti-secretory effects occurring at concentrations which concomitantly reduced barrier function and increased LDH release. These results suggest that the reduction in agonist-stimulated Cl^- secretion from T_{84} cells elicited by compounds **1**–**3** may be due to their toxic effects. While the reductions in Cl^- secretion appear to coincide with increased toxicity, further investigations of this effect would elucidate what components of the Cl^- secretory pathway are being affected by the compounds.

4. Conclusions

In this work we reported the synthesis and characterisation of three iron(III) complexes with ligands derived from *N*-ethyl-*N*-(2-

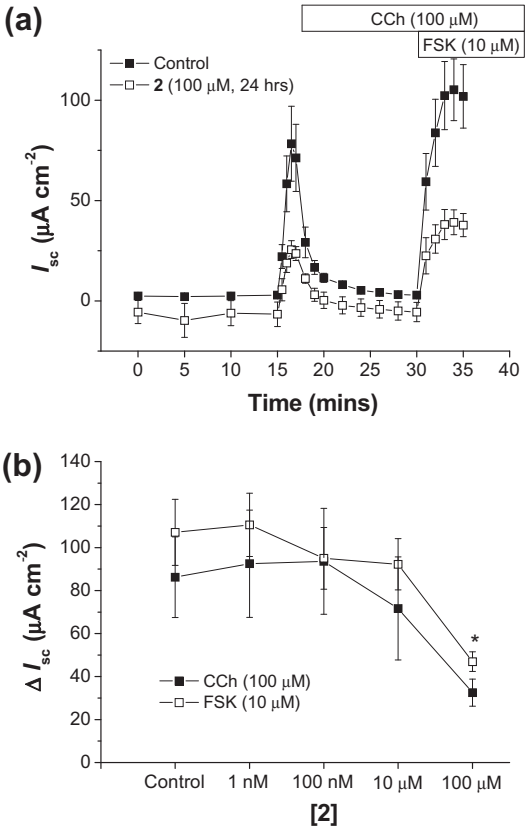

Fig. 9. Compound **2** attenuates Cl^- secretion across T_{84} cells. (a) T_{84} cell monolayers were treated bilaterally with compound **2** (100 μM) in serum- free medium for 24 h. Cells were then washed and mounted in Ussing chambers, and I_{sc} responses to CCh (100 μM) and FSK (10 μM) were measured (n = 6–8). (b) T_{84} monolayers were treated with compound **2** at various concentrations (1 nM to 100 μM) for 24 h before I_{sc} responses to CCh and FSK were measured (n = 6–8).

aminoethyl)salicylaldiminate (H, **1**; 5-Br, **2**; 3-OMe, **3** substituents at the phenyl group).

Investigation of the magnetic behaviour of compounds **1** and **2** in DMSO solutions showed that while compound **1** is predominantly in the HS state, compound **2** shows a mixture of spin states. NMRD measurements showed that scarcely explored Fe(III) complexes reduce the T_1 as commonly observed for other contrast agents. The relaxivity behaviour can be explained by a sum of inner and outer sphere spin-lattice relaxation contributions. Biological assessment of cell toxicity and regulation showed that all three compounds have a toxic effect only at high concentrations (>100 μM), and the effects reflect a reduction in colonic epithelial secretory function.

The hypothesis of association between individual molecules without spin coupling, suggested by the analysis of the spin-lattice relaxation data, will be explored as a future development of the present work.

Finally, we can conclude that, despite the low toxicity, further studies are needed in order to evaluate the potential of these complexes as MRI contrast agents. It would be interesting to translate the NMR studies into a biological medium to assess their MRI potential.

Acknowledgements

We thank Fundação para Ciência e Tecnologia for financial support (UID/MULTI/00612/2013, PEst-OE/QUI/UI0536/2011, PEst-OE/FIS/UI0261/2011, PEst-OE/FIS/UI0261/2014) and fellowships to P.N.M. and S. Barroso (SFRH/BPD/73345/2010 and SFRH/BPD/7394/2010). S. Barroso is grateful to Centro de Química Estrutural for the access to crystallography facilities.

Appendix A. Supplementary material

Supplementary data associated with this article can be found, in the online version, at http://dx.doi.org/10.1016/j.ica.2015.04.026.

References

[1] W. Semmler, M. Schwaiger (Eds.), Molecular Imaging I, Springer, 2008.
[2] T.F. Massoud, S.S. Gambhir, Genes Dev. 17 (2003) 545.
[3] M. Rudin, R. Weissleder, Nat. Rev. Drug Discov. 2 (2003) 123.
[4] D.W. McRobbie, E.A. Moore, M.J. Graves, M.R. Prince, MRI: From Picture to Proton, second ed., Cambridge University Press, New York, 2006.
[5] C.J. Jones, J.R. Thornback, Medicinal Applications of Coordination Chemistry, Royal Society of Chemistry, Cambridge, 2007.
[6] H.S. Thomsen, S.K. Morcos, T. Almén, M.-F. Bellin, M. Bertolotto, G. Bongartz, O. Clement, P. Leander, G. Heinz-Peer, P. Reimer, F. Stacul, A. van der Molen, J.A. Webb, Eur. Radiol. 23 (2013) 307.
[7] Y. Xiao, Y.-J. Wu, W.-J. Zhang, X.-J. Li, F.-K. Pei, J. Anal. Chem. 39 (2011) 757.
[8] S.-P. Lin, J.J. Brown, J. Magn. Reson. Imag. 25 (2007) 884.
[9] T. Grobner, Nephrol. Dial. Transplant. 21 (2006) 1104.
[10] T. Grobner, Nephrol. Dial. Transplant. 21 (2006) 1745.
[11] R. Yacoub, K. Kandukurti, M. Panesar, ISRN Transplant. 2013 (2013) 1.
[12] M.F. Wendland, NMR Biomed. 17 (2004) 581.
[13] A.C. Silva, N.A. Bock, Schizophr. Bull. 34 (2008) 595.
[14] A.G. Roca, R. Costo, A.F. Rebolledo, S. Veintemillas-Verdaguer, P. Tartaj, T. González-Carreño, M.P. Morales, C.J. Serna, J. Phys. D. Appl. Phys. 42 (2009) 224002.
[15] A.C. Silva, J.H. Lee, I. Aoki, A.P. Koretsky, NMR Biomed. 17 (2004) 532.
[16] A. Merbach, L. Helm, E. Tóth, The Chemistry of Contrast Agents in The Chemistry of Contrast Agents in Magnetic Resonance Imaging, second ed., John Wiley & Sons Ltd, 2013.
[17] S.J. Dorazio, J.R. Morrow, Eur. J. Inorg. Chem. 2012 (2012) 2006.
[18] S.J. Dorazio, P.B. Tsitovich, K.E. Siters, J.A. Spernyak, J.R. Morrow, J. Am. Chem. Soc. 133 (2011) 14154.
[19] S.J. Dorazio, J.R. Morrow, Inorg. Chem. 51 (2012) 7448.
[20] P.B. Tsitovich, J.R. Morrow, Inorg. Chim. Acta 393 (2012) 3.
[21] S.J. Dorazio, P.B. Tsitovich, J. Inorg. Biochem. 117 (2012) 212.
[22] D.L. White, Magn. Reson. Med. 312 (1991) 309.
[23] N. Richardson, J.A. Davies, B. Radüchel, Polyhedron 18 (1999) 2457.
[24] D.D. Schwert, N. Richardson, G. Ji, B. Radüchel, W. Ebert, P.E. Heffner, R. Keck, J.A. Davies, J. Med. Chem. 48 (2005) 7482.
[25] P.B. Tsitovich, J.A. Spernyak, J.R. Morrow, Angew. Chem., Int. Ed. Engl. 52 (2013) 13997.
[26] S.J. Dorazio, A.O. Olatunde, J.A. Spernyak, J.R. Morrow, Chem. Commun. (Camb). 49 (2013) 10025.
[27] A.O. Olatunde, S.J. Dorazio, J.A. Spernyak, J.R. Morrow, J. Am. Chem. Soc. 134 (2012) 18503.
[28] C.E. Housecroft, A.G. Sharpe, Inorganic Chemistry, second ed., Pearson Education Limited, 2005.
[29] V. Stavila, M. Allali, L. Canaple, Y. Stortz, C. Franc, P. Maurin, O. Beuf, O. Dufay, J. Samarut, M. Janier, J. Hasserodt, New J. Chem. 32 (2008) 428.
[30] X. Zhao, H. Zhao, Z. Chen, M. Lan, J. Nanosci. Nanotechnol. 14 (2014) 210.
[31] Y. Jun, J.-H. Lee, J. Cheon, Angew. Chem., Int. Ed. Engl. 47 (2008) 5122.
[32] S. Kumar, D.N. Dhar, P.N. Saxena, J. Sci. 68 (2009) 181.
[33] P.N. Martinho, A.I. Vicente, S. Realista, M.S. Saraiva, A.I. Melato, P. Brandão, L.P. Ferreira, M.D. Carvalho, J. Organomet. Chem. 760 (2014) 48.
[34] K.E. Barrett, S.J. Keely, Annu. Rev. Physiol. 62 (2000) 535.
[35] D.F. Evans, J. Chem. Soc. (1959) 2003.
[36] G.M. Sheldrick, SADABS, Empiracal Absorpt. Correct. Program, Univ. Göttingen (1995) based on the methods of Blessing.
[37] M.C. Burla, R. Caliandro, M. Camalli, B. Carrozzini, G.L. Cascarano, L. De Caro, C. Giacovazzo, G. Polidori, R. Spagna, J. Appl. Crystallogr. 38 (2005) 381.
[38] L.J. Farrugia, J. Appl. Crystallogr. 32 (1999) 837.
[39] G. Sheldrick, Göttingen, Ger. (1997).
[40] G.M. Sheldrick, Acta Crystallogr., Sect. A. 64 (2008) 112.
[41] L.J. Farrugia, J. Appl. Crystallogr. 30 (1997) 565.
[42] D.M. Sousa, G.D. Marques, J.M. Cascais, P.J. Sebastião, Solid State Nucl. Magn. Reson. 38 (2010) 36.
[43] W.S. Price, Concepts Magn. Reson. 9 (1997) 299.
[44] J.B.J. Ward, K. Lawler, S. Amu, C.T. Taylor, P.G. Fallon, S.J. Keely, FASEB J. 25 (2011) 535.
[45] C.A. Cartwright, J.A. McRoberts, K.G. Mandel, K. Dharmsathaphorn, J. Clin. Invest. 76 (1985) 1837.
[46] C.N. Field, M. Boillot, R. Clément, J. Mater. Chem. 8 (1998) 283.
[47] C. Faulmann, K. Jacob, S. Dorbes, S. Lampert, I. Malfant, M.L. Doublet, L. Valade, J.A. Real, Inorg. Chem. 46 (2007) 8548.
[48] A. Tissot, R. Bertoni, E. Collet, L. Toupet, M.-L. Boillot, J. Mater. Chem. 21 (2011) 18347.

[49] C. Faulmann, J. Chahine, L. Valade, G. Chastanet, J.-F. Létard, D. de Caro, Eur. J. Inorg. Chem. 2013 (2013) 1058.
[50] C.-F. Sheu, S.-M. Chen, G.-H. Lee, Y.-H. Liu, Y.-S. Wen, J.-J. Lee, Y.-C. Chuang, Y. Wang, Eur. J. Inorg. Chem. 2013 (2013) 894.
[51] Gaussian 09, Revision A.02, M.J. Frisch, G.W. Trucks, H.B. Schlegel, G.E. Scuseria, M.A. Robb, J.R. Cheeseman, G. Scalmani, V. Barone, B. Mennucci, G.A. Petersson, H. Nakatsuji, M. Caricato, X. Li, H.P. Hratchian, A.F. Izmaylov, J. Bloino, G. Zheng, J.L. Sonnenberg, M. Hada, M. Ehara, K. Toyota, R. Fukuda, J. Hasegawa, M. Ishida, T. Nakajima, Y. Honda, O. Kitao, H. Nakai, T. Vreven, J. Montgomery, J. A., J.E. Peralta, F. Ogliaro, M. Bearpark, J.J. Heyd, E. Brothers, K.N. Kudin, V.N. Staroverov, R. Kobayashi, J. Normand, K. Raghavachari, A. Rendell, J.C. Burant, S.S. Iyengar, J. Tomasi, M. Cossi, N. Rega, M.J. Millam, M. Klene, J.E. Knox, J.B. Cross, V. Bakken, C. Adamo, J. Jaramillo, R. Gomperts, R.E. Stratmann, O. Yazyev, A.J. Austin, R. Cammi, C. Pomelli, J.W. Ochterski, R.L. Martin, K. Morokuma, V.G. Zakrzewski, G.A. Voth, P. Salvador, J.J. Dannenberg, S. Dapprich, A.D. Daniels, Ö. Farkas, J.B. Foresman, J. V. Ortiz, J. Cioslowski, D.J. Fox, Gaussian Inc, Wallingford CT, 2009.
[52] J. Perdew, Phys. Rev. B 33 (1986) 8822.
[53] J.P. Perdew, K. Burke, M. Ernzerhof, Phys. Rev. Lett. 78 (1997) 1396.
[54] R. Ditchfield, J. Chem. Phys. 54 (1971) 724.
[55] W.J. Hehre, J. Chem. Phys. 56 (1972) 2257.
[56] P.C. Hariharan, J.A. Pople, Theor. Chim. Acta 28 (1973) 213.
[57] P.C. Hariharan, J.A. Pople, Mol. Phys. 27 (1974) 209.
[58] M.S. Gordon, Chem. Phys. Lett. 76 (1980) 163.
[59] M.F. Tweedle, L.J. Wilson, J. Am. Chem. Soc. 98 (1976) 4824.
[60] E.J. Werner, A. Datta, C.J. Jocher, K.N. Raymond, Angew. Chem., Int. Ed. Engl. 47 (2008) 8568.
[61] P. Gillis, A. Roch, R.A. Brooks, J. Magn. Reson. 137 (1999) 402.
[62] P.J. Sebastião, Eur. J. Phys. 35 (2014) 015017.